Volume 52 March 1987 Number 3

GEOPHYSICS

Magnetotelluric strike rules

P. Zhang*, R. G. Roberts*, and L. B. Pedersen*

ABSTRACT

The distortion of the magnetotelluric impedance tensor by complex "near-surface" structure leads to leakage between the elements of the tensor. The magnetotelluric impedance tensor for our principal model, which has both a local and a regional strike, can be written in the long-period limit as a sum of the regional, undistorted impedance and a perturbed impedance. The latter can be written as a product of a local distortion (which can be regarded as thin-sheet distortion in the long-period range) tensor and the regional impedance.

Local and regional strikes are found by rotating the impedance tensor into directions in which diagonal elements are proportional and column elements are proportional, respectively. The regional impedance tensor is calculated assuming that the strikes are uniquely defined.

An example from a crystalline area with well conducting fracture zones illustrates the model concepts. A weighted least-squares procedure is used for the estimation of distortion parameters.

INTRODUCTION

Magnetotelluric theory as formulated by Cagniard (1953) is based upon a one-dimensional (1-D) model for an Earth structure in which resistivity varies only as a function of depth. In this context only one set of horizontal electrical and perpendicular magnetic components is needed to describe the Earth structure at depth. This model is referred to as the scalar magnetotelluric method.

Seven years later, Cantwell (1960) gave a more general theory to take into account that real Earth structures are seldom adequately described in terms of a stratified model, especially considering that electrical resistivity of natural rocks varies over many orders of magnitude. In Cantwell's description, the signature of a particular measurement site is defined by the impedance tensor, which relates the horizontal magnetic components to the horizontal electrical components at a particular period (and wavenumber of the source field; but this is assumed to be sufficiently planar that only the zero-wavenumber component is needed). The existence and uniqueness of the impedance tensor follow directly from the linearity of Maxwell's equations. The primary magnetic field, which in this approximation is planar and propagating vertically downward to the surface of the Earth, is the source for the electromagnetic (EM) field. The primary field induces electrical fields and magnetic fields which are linearly related to the same primary excitation. Therefore, the total EM fields are themselves linearly related. Thus we can write

$$\begin{bmatrix} E_x(\mathbf{r}, \mathbf{k}, \omega) \\ E_y(\mathbf{r}, \mathbf{k}, \omega) \\ H_z(\mathbf{r}, \mathbf{k}, \omega) \end{bmatrix} = \begin{bmatrix} Z_{xx}(\mathbf{r}, \mathbf{k}, \omega) & Z_{xy}(\mathbf{r}, \mathbf{k}, \omega) \\ Z_{yx}(\mathbf{r}, \mathbf{k}, \omega) & Z_{yy}(\mathbf{r}, \mathbf{k}, \omega) \\ A(\mathbf{r}, \mathbf{k}, \omega) & B(\mathbf{r}, \mathbf{k}, \omega) \end{bmatrix} \begin{bmatrix} H_x(\mathbf{r}, \mathbf{k}, \omega) \\ H_y(\mathbf{r}, \mathbf{k}, \omega) \end{bmatrix}, \quad (1)$$

where $\mathbf{E}$ and $\mathbf{H}$ represent the electric and magnetic fields at the surface, and are functions of frequency ω and wavenumber $\mathbf{k}$ (equal to zero in this context). The subscripts x, y, and z correspond to northward, eastward, and vertical components, respectively.

Manuscript received by the Editor April 28, 1986; revised manuscript received August 8, 1986.
*Uppsala University, Department of Geophysics, Box 556, S-751 22, Uppsala, Sweden.

The 2 × 2 tensor

$$\underline{Z} = \begin{bmatrix} Z_{xx} & Z_{xy} \\ Z_{yx} & Z_{yy} \end{bmatrix}$$

is the MT impedance tensor and (A, B) is the magnetic transfer function introduced by Parkinson (1962). Thus the horizontal magnetic field components can be regarded as the inputs to linear filters $\underline{Z}$ and (A, B) which output the horizontal electric and the vertical magnetic fields.

We recall the following properties of $\underline{Z}$ and (A, B):

for 1-D structure,

$$Z_{xx} = Z_{yy} = 0, \qquad Z_{xy} + Z_{yx} = 0, \qquad A = B = 0;$$

for 2-D structure,

$$Z_{xx} + Z_{yy} = 0, \qquad Z_{xy} + Z_{yx} \neq 0, \qquad A \neq B \neq 0;$$

after rotation of the coordinate system to the strike of the structure,

$$Z_{xx} = Z_{yy} = 0, \qquad A = 0, \qquad B \neq 0;$$

for 3-D structure there are no such constraints. These properties are necessary but not sufficient. For example, 3-D structures exist where $Z_{xx} = Z_{yy} = 0$ and $A = B = 0$ for all periods, but these are exceptions and from a practical point of view the above criteria are also sufficient.

In crystalline areas, large lateral inhomogeneities at the surface are often found, where intact rock blocks are bordered by fracture zones with resistivities typically 100 to 1 000 times smaller than that of the intact rock. This explains why we rarely find cases which have 1-D tensor properties, or even 2-D properties at all periods. Nevertheless, the interpretation and inversion of magnetotelluric (MT) data have almost always been done with 1-D or at most 2-D models. A full 3-D description of the Earth is too complicated and expensive, and also the density of measurement stations is normally too sparse to warrant a detailed modeling exercise.

As an alternative, much effort has been put into approximating the real 3-D Earth by 1-D models, for which there are well-developed inversion schemes (Jupp and Vozoff, 1975; Parker, 1980; Fisher et al., 1981). Different groups seem to use different forms of the impedance tensor for their 1-D inversion. One method finds the strike by antidiagonalizing the impedance tensor and/or by finding the direction where A is zero in some least-squares sense. This is done for all period intervals, whereby different strikes are found for different periods. It is often assumed that these directions define the E-polarization mode, and thus for long periods the above procedure should lead to data sets that are relatively undisturbed by near-surface inhomogeneities. The result will be correct if the defined strike coincides with the strike of the overburden, but unless the regional structure can be well approximated by a 1-D structure, there is no guarantee of such coincidence of the strikes.

Another method uses the strikes as defined above as a function of period to estimate an average strike, which is then kept constant for all periods to define data sets used for formal 1-D inversion or 2-D modeling.

A third approach was introduced by Berdichevskiy and Dmitriev (1976), who suggested using one of the rotationally invariant elements of the impedance tensor for formal inversion:

$$(Z_{xy} - Z_{yx})/2, \tag{2}$$

and

$$(Z_{xx} Z_{yy} - Z_{xy} Z_{yx})^{1/2}. \tag{3}$$

These elements are unique for one particular measuring site irrespective of any complicated inhomogeneity structure in the Earth; they can thus be said to be unbiased by a more or less subjective determination of strikes. While interpretation of these elements in terms of underlying Earth structure can sometimes be grossly misleading, the results of Ranganayaki (1984), for example [who used the form of equation (3) for interpretation of a large number of data sets from a sedimentary area] showed a good internal consistency.

The most recent attempt at deriving consistent strikes was published by Gamble et al. (1982). In essence their method is based upon the idea that with many MT sites distributed over the area of interest, if there is a regional strike, it will be sufficiently stable to survive the influence of randomly distributed strikes of near-surface structures. Gamble et al. estimated the strike using both the tipper and the impedance tensor along three different profiles in a geothermal area at Cerro Prieto, Mexico. While both methods gave stable results, the impedance tensor analysis was superior. Near-surface electrical structures are known to be complex, especially in crystalline regions. Such areas are generally predominantly insulating, with resistivities around $10^4\ \Omega \cdot m$, and they are often intersected by better conducting fracture zones of resistivities of about $100\ \Omega \cdot m$, widths of perhaps several hundred meters, and depths in the kilometer range. Figure 1 shows evidence for fracture zones in a crystalline terrain. The map shows the EM signature in the Siljan impact structure region of central Sweden. An airborne VLF technique with a 16 kHz transmitter at Rugby, England was used. The overburden in the area is normally less than 10 m thick, and it is believed that most of the anomalies can be explained as the effect of the well conducting fracture zones with strikes predominately in the direction of the transmitter, i.e., approximately southwest-northeast. A typical distance between fracture zones seems to be a few kilometers, somewhat closer in the center of the impact structure than outside, where the anomalies seem to be more persistent and wider. In this report we shall make use of a model that reflects the features described above. We divide the structure into a local and a regional structure as shown in Figure 2. The local structure is characterized by a low conductivity σ_1 interrupted by better conducting segments of conductivity σ_2 in a resistive terrain. The regional model may be either 1-D, 2-D or 3-D, but supposedly the scale of conductivity variations at greater depth is much larger than in the local structure, because fractures in the regional part would have a tendency to close under the prevailing lithostatic pressure.

DISTORTION MODEL

The effects of near-surface lateral inhomogeneities on the impedance tensor and geomagnetic transfer functions (tipper) have been treated by Larsen (1975), Babour and Mosnier (1979), Hermance (1982), Le Mouel and Menvielle (1982), and Wannamaker et al. (1984). We use a description similar to that

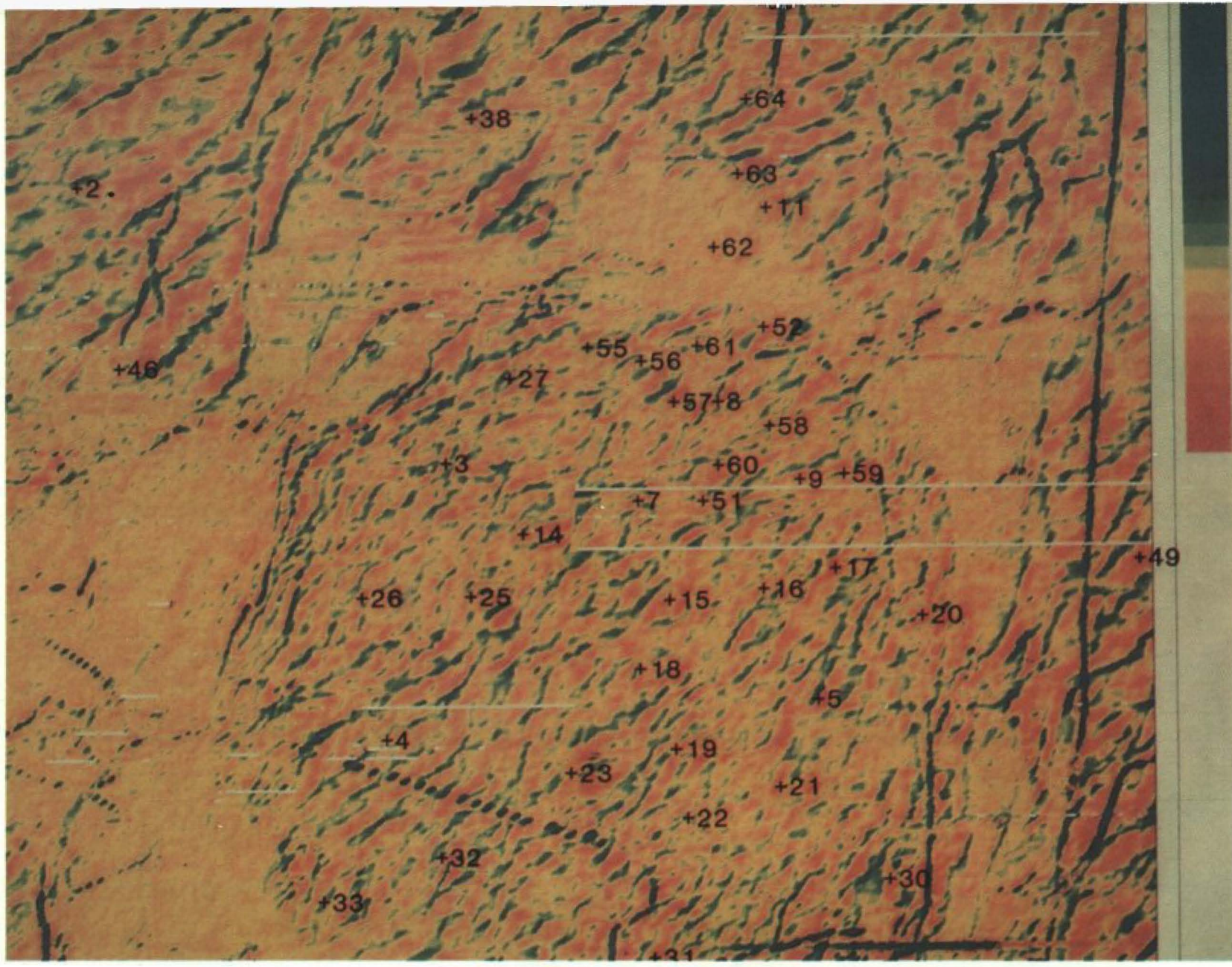

FIG. 1. Airborne VLF map centered on the Siljan impact structure. Transmitter at Rugby, England oriented southwest. Flight altitude and line spacing were 30 m and 200 m, respectively. The color scale corresponds to total field values in steps of 30 promille. The normal field is defined as 1 000 promille. Highly conductive fracture zones and power lines appear as bluish areas. Magnetotelluric stations in the area are denoted by numbers. Station 59, which lies to the northeast, appears to be in the middle of a fracture zone.

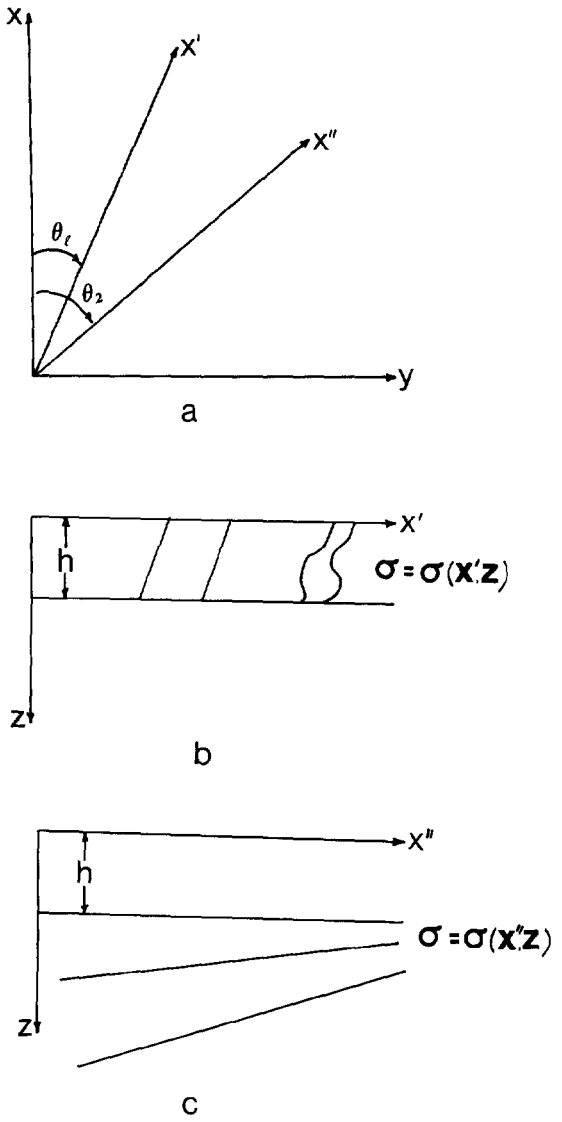

FIG. 2. Geometry of the principal model. (a) Horizontal projection showing the horizontal measurement coordinate system (x, y) with the local strike at azimuth θ_ℓ and the regional strike at azimuth θ_r. (b) Vertical projection through local structure. Thickness h is small compared with the depth of penetration (skin depth). Conductivity distribution is 2-D: $\sigma(x', z)$. (c) Vertical projection through the regional structure. Conductivity distribution is 2-D: $\sigma(x'', z)$.

of Wannamaker et al., modified to include the fact that the regional structure may be 1-D, 2-D, or 3-D. Then the distortion due to local inhomogeneities at the Earth's surface may be expressed as

$$\mathbf{E} = \mathbf{E}^0 + \underset{\sim}{P}^*\mathbf{E}^0; \qquad \mathbf{E}^0 = \mathbf{E}_h^0 + E_z^0\,\mathbf{z}, \tag{4}$$

and

$$\mathbf{H} = \mathbf{H}^0 + \underset{\sim}{Q}^*\mathbf{E}^0; \qquad \mathbf{H}^0 = \mathbf{H}_h^0 + H_z^0\,\mathbf{z}, \tag{5}$$

where $\mathbf{E}^0$ and $\mathbf{H}^0$ denote the EM surface field away from local inhomogeneities. Note that the regional electric and magnetic fields $\mathbf{E}^0$ and $\mathbf{H}^0$ may contain vertical components. $\underset{\sim}{P}^*$ and $\underset{\sim}{Q}^*$ are 3×3 tensors that are essentially constant at periods for which the local structure can be regarded as a thin sheet.

We assume that the source field has only horizontal components (the MT approximation); it follows that at a given period, only two horizontal electric components are necessary to describe any EM field component measured anywhere at the surface. We may take the horizontal electric field $\mathbf{E}_h^0$ to represent these two degrees of freedom. From equation (4) we find

$$\begin{aligned}\mathbf{E} &= \mathbf{E}^0 + \underset{\sim}{P}^*\mathbf{E}^0 \\ &= \mathbf{E}_h^0 + E_z^0\,\mathbf{z} + \underset{\sim}{P}_h^*\mathbf{E}_h^0 + P_{xz}^* E_z^0\,\mathbf{x} + P_{yz}^* E_z^0\,\mathbf{y} + \mathbf{R},\end{aligned}$$

and

$$\mathbf{R} = (P_{zx}^* E_x^0 + P_{zy}^* E_y^0 + P_{zz}^* E_z^0)\mathbf{z}.$$

Defining the geoelectric transfer functions (C^0, D^0) as

$$E_z^0 = C^0 E_x^0 + D^0 E_y^0,$$

and inserting this equation into the former one, we arrive at the following relations between electric horizontal components:

$$\mathbf{E}_h = (\underset{\sim}{I} + \underset{\sim}{P}_h^* + \underset{\sim}{U})\mathbf{E}_h^0,$$

where

$$\underset{\sim}{U} = \begin{bmatrix} C^0 P_{xz}^* & D^0 P_{xz}^* \\ C^0 P_{yz}^* & D^0 P_{yz}^* \end{bmatrix}.$$

We can define an effective distortion tensor $\underset{\sim}{P}_h$ as $\underset{\sim}{P}_h = \underset{\sim}{P}_h^* + \underset{\sim}{U}$, to get the simple relation

$$\mathbf{E}_h = (\underset{\sim}{I} + \underset{\sim}{P}_h)\mathbf{E}_h^0.$$

Similarly, from equation (5),

$$\begin{aligned}\mathbf{H} &= \mathbf{H}^0 + \underset{\sim}{Q}^*\mathbf{E}^0 \\ &= \mathbf{H}_h^0 + H_z^0\,\mathbf{z} + \underset{\sim}{Q}_h^*\mathbf{E}_h^0 + Q_{xz}^* E_z^0\,\mathbf{x} + Q_{yz}^* E_z^0\,\mathbf{y} + \mathbf{T}\end{aligned}$$

where

$$\mathbf{T} = (Q_{zx}^* E_x^0 + Q_{zy}^* E_y^0 + Q_{zz}^* E_z^0)\mathbf{z}.$$

The relation between magnetic horizontal components can be written

$$\mathbf{H}_h = \mathbf{H}_h^0 + (\underset{\sim}{Q}_h^* + \underset{\sim}{V})\mathbf{E}_h^0,$$

where

$$\underset{\sim}{V} = \begin{bmatrix} C^0 Q_{xz}^* & D^0 Q_{xz}^* \\ C^0 Q_{yz}^* & D^0 Q_{yz}^* \end{bmatrix},$$

which allows us to define an effective distortion tensor $\underset{\sim}{Q}_h$ as

$\underset{\sim}{Q}_h = \underset{\sim}{Q}_h^* + \underline{Y}$. This leads to the following expression:

$$H_h = (\underline{I} + \underset{\sim}{Q}_h \underset{\sim}{Z}^0)\mathbf{H}_h^0.$$

This finally gives an expression for the distorted impedance tensor $\underset{\sim}{Z}$ where $\mathbf{E}_h = \underset{\sim}{Z}\mathbf{H}_h$, in terms of the undistorted impedance tensor $\underset{\sim}{Z}^0$, where $\mathbf{E}_h^0 = \underset{\sim}{Z}^0\mathbf{H}_h^0$, as

$$\underset{\sim}{Z} = (\underline{I} + \underline{P}_h)\underset{\sim}{Z}^0(\underline{I} + \underset{\sim}{Q}_h \underset{\sim}{Z}^0)^{-1}. \tag{6}$$

The magnetic transfer function is defined as

$$H_z = AH_x + BH_y = (A, B)\mathbf{H}_h.$$

Thus the vertical magnetic field can be related to $\mathbf{E}_h^0$ through the undistorted magnetic transfer function (A^0, B^0) as

$$H_z = H_z^0 + (Q_{zx}^* + Q_{zz}^* C^0, Q_{zy}^* + Q_{zz}^* D^0)\mathbf{E}_h^0$$
$$= \left[(A^0, B^0) + (Q_{zx}, Q_{zy})\underset{\sim}{Z}^0\right]\mathbf{H}_h^0,$$

where $Q_{zx} = Q_{zx}^* + Q_{zz}^* C^0$ and $Q_{zy} = Q_{zy}^* + Q_{zz}^* D^0$ are effective distortion parameters. Finally, the magnetic transfer functions (A, B) can be written

$$(A, B) = \left[(A^0, B^0) + (Q_{zx}, Q_{zy})\underset{\sim}{Z}^0\right](\underline{I} + \underset{\sim}{Q}_h \underset{\sim}{Z}^0)^{-1}. \tag{7}$$

In the low-frequency (long-period) limit, $|\underset{\sim}{Z}^0|$ decays as the inverse square root of the period. Approximately,

$$\underset{\sim}{Z} \approx (\underline{I} + \underline{P}_h)\underset{\sim}{Z}^0, \tag{8}$$

and

$$(A, B) \approx (A^0, B^0). \tag{9}$$

Thus the magnetic field vector will be relatively free of distortions caused by the local structure, whereas the electrical field vector will be distorted by a real tensor.

In the following we investigate our principal distortion model with regard to finding strikes and possibly correcting the measured impedance tensor to retrieve the regional tensor.

The principal model is shown in Figure 2. The local structure is assumed to be 2-D with a strike θ_ℓ. The regional structure is also 2-D, but with a different strike, θ_r. The local structure is fully described by three real parameters (P_{xx}, P_{yy}, and θ_ℓ). However, P_{xx} or P_{yy} will be approximately equal to zero, because currents flowing parallel to the strike will not produce charges at discontinuities in conductivities. The local structure will thus be transparent to an electrical field in that direction.

In an arbitrary direction away from θ_ℓ, the distortion tensor can be expressed as

$$\underline{P}_h(\theta - \theta_\ell) = \underline{R}(\theta - \theta_\ell)\begin{bmatrix} P_{xx} & 0 \\ 0 & P_{yy} \end{bmatrix}\underline{R}^T(\theta - \theta_\ell)$$
$$= P_1\underline{I} + P_2\left[\mathbf{V}_1(\theta - \theta_\ell), \mathbf{V}_2(\theta - \theta_\ell)\right], \tag{10}$$

with

$$\underline{R}(\theta - \theta_\ell) = \begin{bmatrix} \cos(\theta - \theta_\ell) & \sin(\theta - \theta_\ell) \\ -\sin(\theta - \theta_\ell) & \cos(\theta - \theta_\ell) \end{bmatrix},$$

$$\mathbf{V}_1 = \begin{bmatrix} \cos 2(\theta - \theta_\ell) \\ -\sin 2(\theta - \theta_\ell) \end{bmatrix},$$

$$\mathbf{V}_2 = \begin{bmatrix} \sin 2(\theta - \theta_\ell) \\ \cos 2(\theta - \theta_\ell) \end{bmatrix},$$

$$P_1 = (P_{xx} + P_{yy})/2,$$

and

$$P_2 = (P_{xx} - P_{yy})/2.$$

Superscript T denotes transposition. Similarly, the regional impedance $\underset{\sim}{Z}^0$ can be expressed as a function of the angle $(\theta - \theta_r)$:

$$\underset{\sim}{Z}^0(\theta - \theta_r) = \underline{R}(\theta - \theta_r)\begin{bmatrix} 0 & Z_{xy}^0 \\ Z_{yx}^0 & 0 \end{bmatrix}\underline{R}^T(\theta - \theta_r)$$
$$= Z_4^0\underline{J} + Z_3^0\left[\mathbf{V}_2(\theta - \theta_r), \mathbf{V}_1(\theta - \theta_r)\right], \tag{11}$$

with

$$Z_3^0 = (Z_{xy}^0 + Z_{yx}^0)/2,$$
$$Z_4^0 = (Z_{xy}^0 - Z_{yx}^0)/2,$$

and

$$\underline{J} = \begin{bmatrix} 0 & 1 \\ -1 & 0 \end{bmatrix}.$$

Local structure

The impedance in the direction of the local strike has a particularly simple structure:

$$\underset{\sim}{Z}(\theta = \theta_\ell)$$
$$= \begin{bmatrix} -(1 + P_{xx})Z_3^0 \sin 2\Delta\theta & (1 + P_{xx})(Z_4^0 + Z_3^0 \cos 2\Delta\theta) \\ (1 + P_{yy})(-Z_4^0 + Z_3^0 \cos 2\Delta\theta) & (1 + P_{yy})Z_3^0 \sin 2\Delta\theta \end{bmatrix}, \tag{12}$$

where $\Delta\theta = \theta_r - \theta_\ell$. Note that the diagonal elements are related to each other by a real constant, i.e.,

$$Z_{xx}(\theta_\ell) = \alpha Z_{yy}(\theta_\ell), \tag{13}$$

with

$$\alpha = -\frac{1 + P_{xx}}{1 + P_{yy}}. \tag{14}$$

If the local strike coincides with the x-axis, then $P_{xx} = 0$. For measurements in a resistive terrain on a conductive inhomogeneity, we expect $-1 < P_{yy} < 0$, since the electric field will be reduced but will not change signs. Thus $\alpha < -1$. With the local strike in the y-direction, we should find $-1 < \alpha < 0$.

For measurements in a conductive terrain on a resistive inhomogeneity, we expect $P_{yy} > 0$, since the electric field will be amplified; thus $-1 < \alpha < 0$. With the local strike in the y-direction, we should find $\alpha < -1$.

Comparison with conventional strike determination

We recall the general expressions for rotated impedance elements:

$$Z_{xx}(\theta) = Z_1 + Z_2 \cos 2\theta + Z_3 \sin 2\theta,$$
$$Z_{yy}(\theta) = Z_1 - Z_2 \cos 2\theta - Z_3 \sin 2\theta,$$
$$Z_{xy}(\theta) = Z_4 + Z_3 \cos 2\theta - Z_2 \sin 2\theta, \quad (15)$$

and

$$Z_{yx}(\theta) = -Z_4 + Z_3 \cos 2\theta - Z_2 \sin 2\theta,$$

where θ is the rotation angle measured clockwise from the measuring directions, and Z_i ($i = 1, \ldots, 4$) are defined as

$$Z_1 = (Z'_{xx} + Z'_{yy})/2,$$
$$Z_2 = (Z'_{xx} - Z'_{yy})/2,$$
$$Z_3 = (Z'_{xy} + Z'_{yx})/2,$$

and

$$Z_4 = (Z'_{xy} - Z'_{yx})/2.$$

The prime indicates the data in the measuring direction.

In a conventional analysis the strike is determined by minimizing $|Z_{xx}(\theta) - Z_{yy}(\theta)|^2$, as proposed by Sims and Bostick (1969). An analytically simpler result can be obtained by the following argument. If the structure were truly 2-D, the strike could be determined from the condition

$$Z_{xx}(\theta) - Z_{yy}(\theta) = 0,$$

leading to a solution for the strike θ_s of

$$\tan 2\theta_s = -\frac{Z'_{xx} - Z'_{yy}}{Z'_{xy} + Z'_{yx}}.$$

Although in general this equation will not give a real solution, we can force it to be real by retrieving only the real part, i.e.,

$$\tan 2\theta_s = -\frac{\mathrm{Re}\left[(Z'_{xy} + Z'_{yx})^*(Z'_{xx} - Z'_{yy})\right]}{|Z'_{xy} + Z'_{yx}|^2}, \quad (16)$$

where the asterisk denotes complex conjugation. We show how the strike determined from this definition deviates from the true strike of the local structure. Inserting the impedance structure given by equation (12) into equation (16) yields, under the assumptions that $P_{xx} \approx 0$ and $P_{yy} \approx -1$,

$$\tan 2\theta_s = \mathrm{Re}\,\frac{\sin 2\Delta\theta Z_3^0}{Z_4^0 + \cos 2\Delta\theta Z_3^0} \approx \frac{S \sin 2\Delta\theta}{1 + S \cos 2\Delta\theta}, \quad (17)$$

where we define the skew as the ratio $S = |Z_3^0|/|Z_4^0| < 1$ and assume that the phase of Z_3^0 and Z_4^0 are approximately the same. An analysis of formula (17) reveals that θ_s will be biased strongly toward the local strike. For instance, if the difference between regional and local strike is 30 degrees and $S = 0.2$, then θ_s is found to be 4.5 degrees, i.e., quite close to the local strike.

Regional strike

Next we consider the form of the total impedance tensor when measured in the direction of the regional strike. For $0 = \theta_r$,

$$\underline{\mathbf{Z}}(\theta_r) = \begin{bmatrix} -P_2 \sin 2\Delta\theta Z_{yx}^0 & (1 + P_1 + P_2 \cos 2\Delta\theta) Z_{xy}^0 \\ (1 + P_1 - P_2 \cos 2\Delta\theta) Z_{yx}^0 & -P_2 \sin 2\Delta\theta\, Z_{xy}^0 \end{bmatrix}. \quad (18)$$

Thus the column elements are related by real constants β and γ:

$$\underline{\mathbf{Z}}(\theta_r) = \begin{bmatrix} \beta Z_{yx} & Z_{xy} \\ Z_{yx} & \gamma Z_{xy} \end{bmatrix}, \quad (19)$$

where

$$\beta = \frac{-P_2 \sin 2\Delta\theta}{1 + P_1 - P_2 \cos 2\Delta\theta}, \quad (20a)$$

and

$$\gamma = \frac{-P_2 \sin 2\Delta\theta}{1 + P_1 + P_2 \cos 2\Delta\theta}. \quad (20b)$$

Within the framework of the principal model of Figure 2, P_1 and P_2 are dependent quantities. Consider the case $P_{xx} = 0$ and $P_{xy} \neq 0$; then $P_1 = -P_2$ and $P_{yy} = -2P_2$. We may now find P_{yy} from equation (20a) or equation (20b),

$$P_{yy}^{\beta} = -\frac{\beta}{2\left[\beta(\cos 2\Delta\theta - 1) - \sin 2\Delta\theta\right]},$$

and

$$P_{yy}^{\gamma} = \frac{\gamma}{2\left[\gamma(1 + \cos 2\Delta\theta) - \sin 2\Delta\theta\right]}.$$

Requiring $P_{yy}^{\beta} = P_{yy}^{\gamma}$ imposes the constraint between the "measured" quantities β, γ, and $\Delta\theta$,

$$\tan 2\Delta\theta = \frac{2\beta\gamma}{\gamma - \beta}. \quad (21)$$

Theoretically, the regional impedance tensor may now be calculated from equations (19) as

$$Z_{xy}^0 = \frac{Z_{xy}}{1 + 0.5P_{yy}(1 - \cos 2\Delta\theta)} = \frac{Z_{xy}}{1 + P_{yy} \sin^2 \Delta\theta}, \quad (22a)$$

and

$$Z_{yx}^0 = \frac{Z_{yx}}{1 + 0.5P_{yy}(1 + \cos 2\Delta\theta)} = \frac{Z_{yx}}{1 + P_{yy} \cos^2 \Delta\theta}. \quad (22b)$$

Strike determinations for models other than the principal model

The total impedance tensor is generally expressed through equation (8). $\underline{\mathbf{P}}$ is the matrix of local distortion with real constants P_{xx}, P_{xy}, P_{yx}, and P_{yy} and $\underline{\mathbf{Z}}^0$ is the undistorted regional impedance. For the principal model, both the local

and regional structures were considered to be 2-D. We briefly consider deviations from that model.

3-D regional structure and 2-D local structure.—In the local coordinate system,

$$\underline{Z}(\theta_\ell) = \begin{bmatrix} Z^0_{xx} & Z^0_{xy} \\ (1 + P_{yy})Z^0_{yx} & (1 + P_{yy})Z^0_{yy} \end{bmatrix}.$$

The local strike cannot be found from strictly theoretical arguments. However, in extreme cases P_{yy} will be either much larger than 1 or close to -1. In the former case, a minimization of the power in the second row with respect to rotation angle will give an approximate determination of θ_ℓ. In the latter case, a maximization of the same power will give an approximate determination of θ_ℓ.

2-D regional structure and 3-D local structure.—In the regional coordinate system,

$$\underline{Z}(\theta_r) = \begin{bmatrix} P_{xy}Z^0_{yx} & (1 + P_{xx})Z^0_{xy} \\ (1 + P_{yy})Z^0_{yx} & P_{yx}Z^0_{xy} \end{bmatrix}.$$

Thus, we may define β and γ as in our principal model to find the regional strike. However, we cannot correct for distortion effects because we cannot make reasonable assumptions about the matrix $\underline{P}$.

3-D or 1-D regional structure and 1-D to 3-D local structure.—Because none of the cases poses either local or regional strike, there is no theoretical basis for preferring one or the other method to determine a direction of currents.

LEAST-SQUARES ESTIMATION OF DISTORTION PARAMETERS

With noise-free data and a consistent principal model, equations (13) and (19) give the "exact" relations:

$$Z_{xx}(\theta_\ell) = \alpha Z_{yy}(\theta_\ell), \tag{23a}$$

$$Z_{xx}(\theta_r) = \beta Z_{yx}(\theta_r), \tag{23b}$$

and

$$Z_{yy}(\theta_r) = \gamma Z_{xy}(\theta_r), \tag{23c}$$

which are valid for all periods exceeding some lower limit, where α, β, γ, θ_ℓ, and θ_r are real constants. Real data are noisy and the real Earth is more complicated than described by the principal model. The diagonal elements Z_{xx} and Z_{yy} are generally the most noisy components of the impedance tensor, simply because they are usually numerically smaller than off-diagonal elements. In our least-squares estimation procedure, we have tried to allow for these conditions by assuming Z_{yx} and Z_{xy} to be noise-free compared with Z_{xx} and Z_{yy}, respectively, and by assuming that the noise levels in Z_{xx} and Z_{yy} are equal.

For each period, interval estimates $\hat{\alpha}$, $\hat{\beta}$, $\hat{\gamma}$, $\hat{\theta}_1$, and $\hat{\theta}_r$ can then be determined by minimizing the target functions:

$$\begin{aligned} Q &= Q(\beta, \gamma, \theta) \\ &= Q_1 + Q_2 \\ &= |\mathbf{Z}^*_{xx} - \beta \mathbf{Z}^*_{yx}|^2 + |\mathbf{Z}^*_{yy} - \gamma \mathbf{Z}^*_{xy}|^2, \end{aligned} \tag{24}$$

and

$$\begin{aligned} Q_3 &= Q_3(\alpha, \theta) \\ &= |\alpha_1 \mathbf{Z}^*_{xx} + \alpha_2 \mathbf{Z}^*_{yy}|^2 + \lambda(1 - \alpha_1^2 - \alpha_2^2); \qquad \alpha = -\alpha_2/\alpha_1, \end{aligned} \tag{25}$$

where impedance vectors with asterisks, $\mathbf{Z}^*_{xx}$, $\mathbf{Z}^*_{yy}$, $\mathbf{Z}^*_{xy}$, and $\mathbf{Z}^*_{yx}$, denote realizations over some specified period interval (for instance, one decade), multiplied by weights inversely related to the standard errors of $Z_{xx}(\theta)$, and λ is a Lagrangian multiplier. From equation (15), the variance of $Z_{xx}(\theta)$ is approximately

$$\begin{aligned} \text{var}\left[Z_{xx}(\theta)\right] \approx\ & \text{var}\,(Z_1) + \text{var}\,(Z_2)\cos^2(2\theta) \\ & + \text{var}\,(Z_3)\sin^2(2\theta), \end{aligned} \tag{26}$$

where

$$\begin{aligned} \text{var}\,(Z_1) &\approx \text{var}\,(Z_{xx})/4 + \text{var}\,(Z_{yy})/4, \\ \text{var}\,(Z_2) &\approx \text{var}\,(Z_1), \\ \text{var}\,(Z_3) &\approx \text{var}\,(Z_{xy})/4 + \text{var}\,(Z_{yx})/4, \end{aligned}$$

and

$$\text{var}\,(Z_4) \approx \text{var}\,(Z_3).$$

In equation (25) we chose to minimize the distance from the regression line $(\alpha_1 Z^*_{xx} + \alpha_2 Z^*_{yy})(\alpha_1^2 + \alpha_2^2)^{-1/2}$ rather than the vertical distance as in equation (24), since Z_{xx} and Z_{yy} are assumed to have the same variances. We are seeking a less biased estimate of α.

For any fixed coordinate frame, Q_1, Q_2, and Q_3 will attain their minima for the following values of $\hat{\beta}$, $\hat{\gamma}$, and $\hat{\alpha}$:

$$\hat{\beta} = \frac{\tilde{\mathbf{Z}}^*_{xx}\mathbf{Z}^*_{yx}}{|\mathbf{Z}^*_{yx}|^2}, \tag{27a}$$

$$\hat{\gamma} = \frac{\tilde{\mathbf{Z}}^*_{yy}\mathbf{Z}^*_{xy}}{|\mathbf{Z}^*_{xy}|^2}, \tag{27b}$$

where a tilde and asterisk mean transposition and complex conjugation, and

$$\hat{\alpha} = -\frac{\hat{\alpha}_1}{\hat{\alpha}_2}, \tag{27c}$$

with

$$\hat{\alpha}_1 = \left\{1 + \left[(S_1 - \lambda^{\pm})/S_3\right]^2\right\}^{-1/2},$$

$$\hat{\alpha}_2 = -\alpha_1(S_1 - \lambda^{\pm})/S_3,$$

$$\lambda^{\pm} = \left\{S_1 + S_2 \pm \left[(S_1 - S_2)^2 + 4S_3^2\right]^{1/2}\right\}/2,$$

$$S_1 = |\mathbf{Z}^*_{xx}|^2, \qquad S_2 = |\mathbf{Z}^*_{yy}|^2,$$

and

$$S_3 = \text{Re}\,(\tilde{\mathbf{Z}}^*_{xx}\mathbf{Z}^*_{yy}).$$

λ is set equal to λ^+ and λ^-. The value which produces the smallest value of Q_3 is the best value.

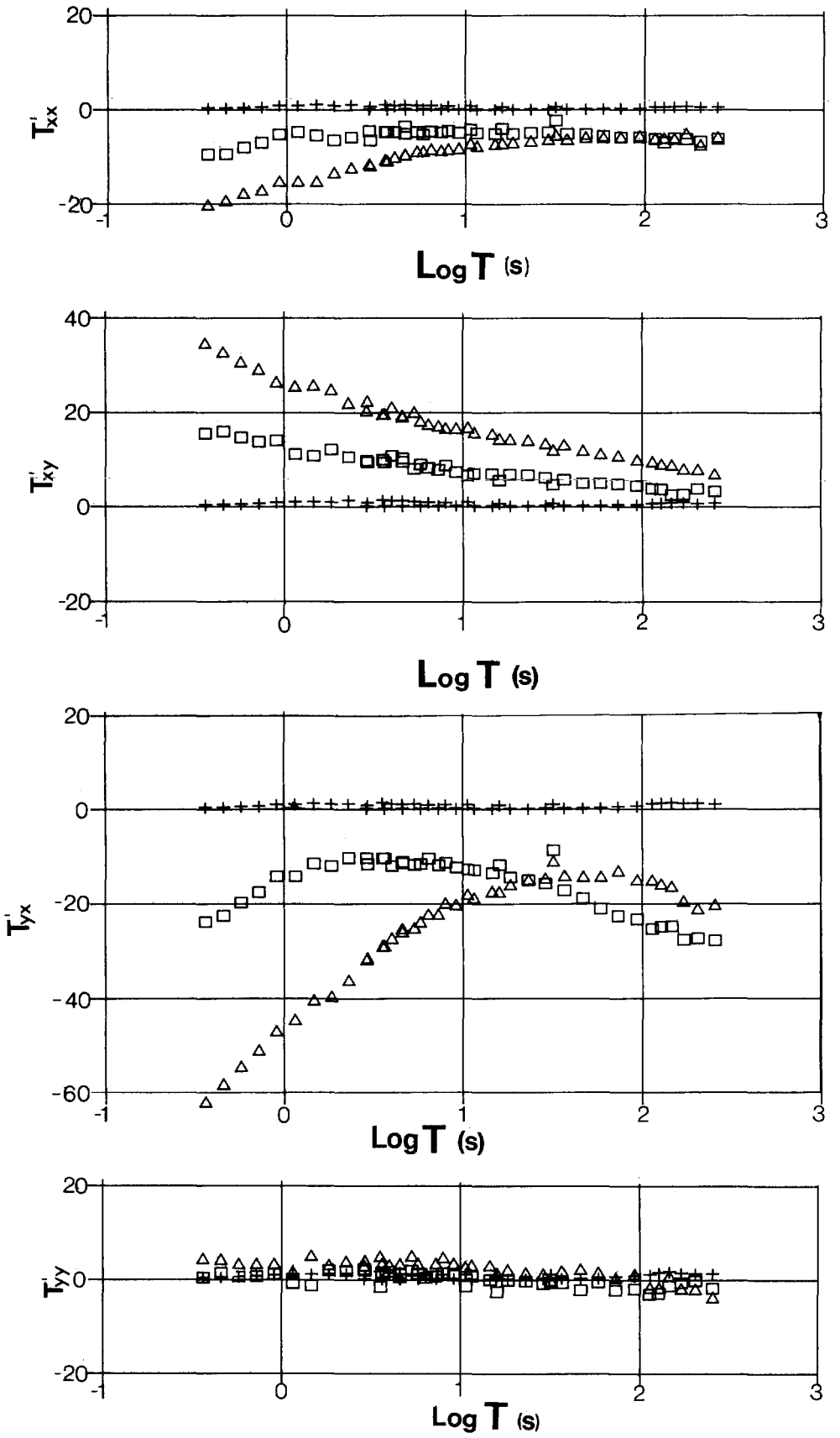

FIG. 3. Estimated impedance tensor at station 59 plotted as a function of period (ten estimates per decade). $\underline{T} = (2\pi/\text{period} \cdot \mu_0)^{-1/2}\underline{Z}$. □: real part; △: imaginary part; +: standard error. (a) T_{xx}; (b) T_{xy}; (c) T_{yx}; (d) T_{yy}.

The global minima of Q and Q_3 may then be found by searching through the interval 0 to 90 degrees in small steps and searching around the minimum points with some interpolation procedure to define the minima better.

Estimation of confidence limits on $\hat{\alpha}$, $\hat{\beta}$, $\hat{\gamma}$, $\hat{\theta}_r$, and $\hat{\theta}_l$

Assume that the global minima of the functions $Q = Q(\theta, \beta, \gamma)$ and $Q_3 = Q_3(\theta, \alpha)$ have been properly defined by the procedure outlined above and denote the minima by Q^0 and Q_3^0, respectively.

The object functions Q and Q_3 are nonquadratic functions of the independent variables, and thus we can only give approximate estimates of the confidence limits. We first assume linearity of models and normal distribution of data errors. Then the value of Q corresponding to a $(1 - \delta)$ 100 percent confidence limit for a parameter will be related to the minimum values Q^0 and Q_3^0 through (Sheffe, 1959)

$$\Delta Q = Q - Q^0 = Q^0 F(1, N - P, 1 - \delta)/(N - P). \quad (28a)$$

The expression for $Q_3 - Q_3^0$ is similar. Here $N - P$ is the effective number of degrees of freedom, i.e., twice the number of frequencies in the period interval under consideration minus the number of parameters in the model. Typically, $N = 20$ and $P = 3$ for Q, and $P = 2$ for Q_3. With these values of N and P, we may approximate the Fischer distribution function F by 1 when $\delta = 0.32$. The 68 percent confidence limit or standard error on, say, θ_r can thus be calculated as the maximum deviation of

$$\Delta\theta_r = |\theta - \theta_r|,$$

under the constraint

$$\Delta Q \leq Q - Q^0 = Q^0/(N - P). \quad (28b)$$

$\Delta\theta_r$ attains its maximum value for $\Delta Q = Q^0/(N - P)$. The problem of finding the confidence limit for θ_r (and θ_l) is now reduced to finding values of Q from a table of local minima as described by equations (27) and interpolating between given values to find the $\Delta\theta_r$ which reproduces $\Delta Q = Q^0/(N - P)$ from equation (28b).

Confidence limits for $\hat{\alpha}$, $\hat{\beta}$, and $\hat{\gamma}$ are found from a linearization of equations (23) around the global minima. However, since $(\beta, \gamma, \theta_r)$ and (α, θ_l) enter into the equations in a highly nonlinear fashion, we have chosen to improve the estimated confidence limits by a procedure described by Johansen (1977) and Pedersen (1979). The procedure is essentially a line search along the direction predicted from the linearized problem until the criterion on ΔQ is fulfilled.

AN EXAMPLE

We show the results of analysis from station 59 in the northeastern part of the map (Figure 1). The VLF results indicate that the station lies on a conductive zone running northeast. However, because of the direction to the relevant transmitter, any zone striking approximately northwest will appear to the VLF as normal crust. The VLF measurements used a source frequency of 16 kHz, and therefore the penetration was only 100–200 m. Fracture zones are expected to be open and fluid-filled (thus well conducting), down to depths of 1–2 km. It follows that local strikes determined from MT data can deviate considerably from VLF strikes.

The impedance tensor is shown in Figure 3 with ten estimates per decade. The x-axis points to magnetic north, and the magnetic declination is approximately -1.5 degrees. The tensor clearly has a 3-D signature with skew values around 0.2 and strong correlations between column elements. The regional strike $\hat{\theta}_r$, local strike $\hat{\theta}_l$, and $\hat{\beta}$, $\hat{\gamma}$, and $\hat{\alpha}$ were estimated over period intervals of one decade and plotted as functions of period (Figures 4 and 5). The regional strike $\hat{\theta}_r$ and distortion parameters $\hat{\beta}$ and $\hat{\gamma}$ are relatively stable from 1 s to 100 s. The local strike $\hat{\theta}_l$ and corresponding scaling parameter α are more scattered, as expected. The conventional strike θ_s deviates considerably from both $\hat{\theta}_l$ and $\hat{\theta}_r$. Note that $\tan^{-1}\hat{\alpha} \approx -70$ degrees, or $\hat{\alpha} = -2$, i.e., the condition $\hat{\alpha} < -1$ is well met. The normalized object functions $Q^0/(N - P)$ and $Q_3^0/(N - P)$ averaged over two decades would be expected to be about 1 if the basic model is correct and if the weighting factors are realistic expressions of the errors of the impedance elements. In the case of station 59, both $Q^0/(N - P)$ and

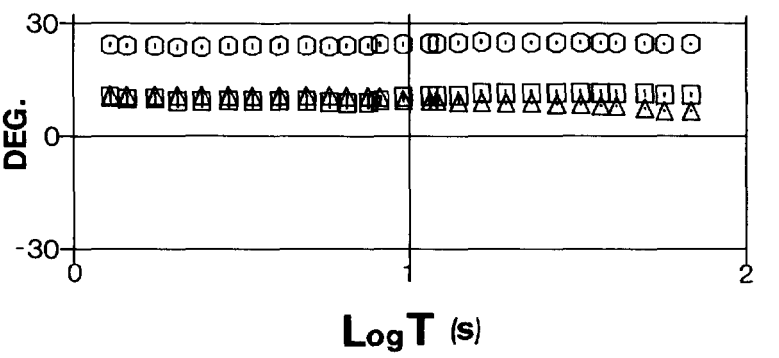

FIG. 4. Estimated distortion parameters as a function of period in the regional coordinate system. Estimates obtained as averages over one decade. □: θ_r; ○: $\tan^{-1}\beta$; and △: $\tan^{-1}\gamma$. Standard errors are denoted by vertical lines.

$Q_3^0/(N-P)$ are around 10–20, which means that the principal model should be rejected if the weighting factors are correct.

Conversely we may accept the principal model if the weighting factors are too big, i.e., the estimated errors on the impedance elements are too small. We have reason to believe that the standard errors are underestimated since they were calculated assuming that the horizontal magnetic field components are noise-free, as described in Pedersen (1982). Instead of using statistical measures to judge whether the model should be rejected as incompatible with the data, we prefer to look more qualitatively on the stability of the estimates. For example, in Figure 4, $\hat{\theta}_r$, $\hat{\beta}$, and $\hat{\gamma}$ are nearly constant as a function of period. This is a necessary condition for a 2-D regional structure and a general 3-D local structure. In this case it seems that the concept of a regional strike is viable. The concept of a local strike seems also to be valid, judging from the stability of $\hat{\theta}_l$ and $\hat{\alpha}$ (Figure 5) and from the value of α being considerably smaller than -1.

The object functions Q and Q_3 usually have rather deep minima, and the calculated errors on $\hat{\theta}_l$ and $\hat{\theta}_r$ are correspondingly small. When all station 59 data from 1 to 100 s have been included, the errors on $\hat{\theta}_l$ and $\hat{\theta}_r$ are ± 2.7 and ± 4.1 degrees, respectively.

The predicted diagonal tensor elements are compared with the measured tensor elements in Figure 6. Note that this best prediction defines the regional strike. The prediction is nearly perfect for Z_{xx}, whereas for Z_{yy} there is greater scatter due to larger scatter in the original data in that direction.

Station 59 is right on the highly conductive fracture zone as shown in Figure 1; considering that α is less than -1, that makes the correction of the impedance tensor possible. As discussed, we can put $P_{xx} = 0$. This allows, from equations (20), the estimation of P_{yy} with less error since $P_{yy} = -0.72$. We can then retrieve the regional impedance tensor according to equations (22) by different scaling factors, i.e., by multiplying Z_{xy} by 1.1 to get Z_{xy}^0 and Z_{yx} by 2.6 to get Z_{yx}^0, respectively.

CONCLUSIONS

The principal model consists of a 2-D local structure underlain by another 2-D regional structure with a different strike. Strikes are denoted by angles θ_ℓ and θ_r, respectively. The model is valid at periods for which the local structure can be regarded as a "thin sheet" (the dc limit).

The regional strike is characterized by that direction where elements of the column of the impedance tensor are proportional. The proportionality constants $\beta = Z_{xx}/Z_{yx}$ and $\gamma = Z_{yy}/Z_{xy}$ are real and independent of period.

The local strike is characterized by that direction where diagonal elements are proportional. The proportionality constant $\alpha = Z_{xx}/Z_{yy}$ is real, negative, and independent of period.

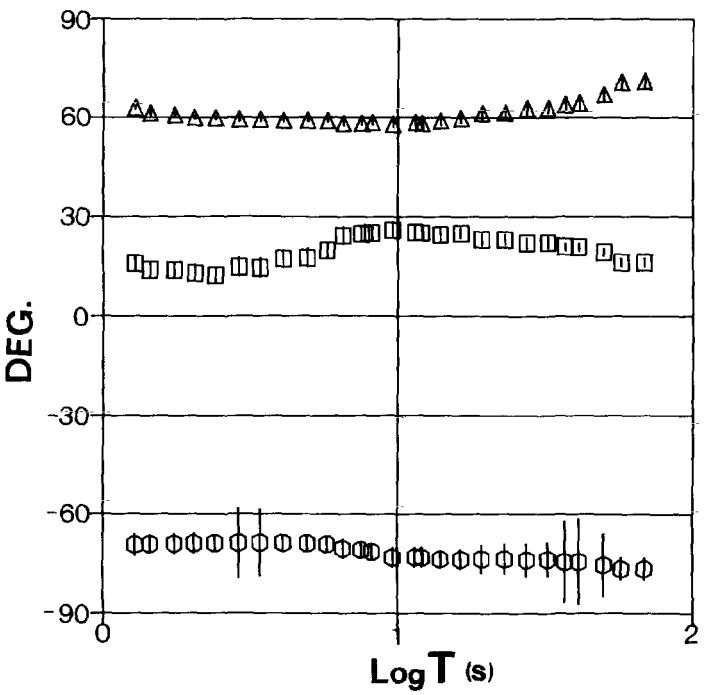

FIG. 5. Estimated distortion parameters as a function of period in the local coordinate system. Estimates obtained as averages over one decade. □: θ_ℓ; ○: $\tan^{-1}\alpha$; and △: θ_s. Standard errors are denoted by vertical lines.

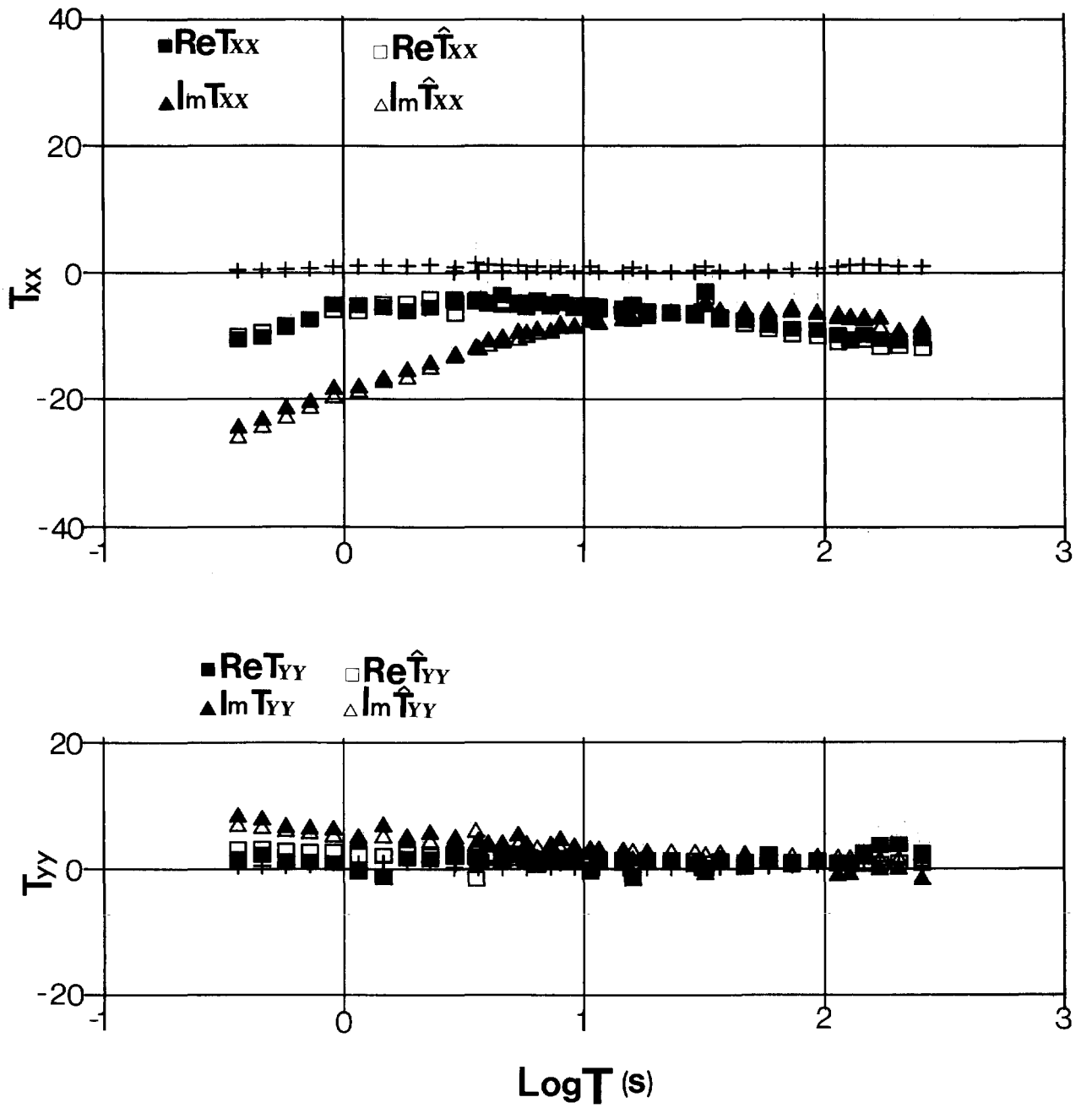

FIG. 6. Comparison between predicted (in black) and "measured" (open) impedance tensors at $\theta_r = 10.7$ degrees as a function of period. □: real part; △: imaginary part; +: standard error. (a) T_{xx}; $\beta = 0.45$. (b) T_{yy}; $\gamma = 0.19$.

Constants β, γ, and θ_r may be defined even for a general local structure, whereas α and θ_ℓ may only be defined for the principal model. The conventional method of strike determination is found to be biased toward the local strike. The inverse problem, i.e., finding strikes, is not entirely unique. Strikes are ambiguous by a factor of $\pi/2$. However, the local strike may be uniquely defined under extreme geoelectric conditions, for example, a highly conductive inhomogeneity embedded in an insulating overburden.

The regional strike can be uniquely defined by adding extra information, either from geologic considerations or from tipper strikes, which uniquely define the regional strike under the assumption of a 2-D regional structure.

The example presented from the Siljan impact structure gives some credence to the applicability of the principal model. Least-squares estimations of distortion parameters (θ_r, β, γ) and (θ_ℓ, α) are found to be relatively stable over the period interval of 1 to 100 s. More work is needed to investigate the wider applicability of the principal model, both in crystalline terrain and in sedimentary environments.

ACKNOWLEDGMENTS

The Swedish Geological Survey is acknowledged for permitting us to publish the VLF map of the Siljan area. Part of this work was carried out with financial support of the Swedish Natural Science Research Council under contract G-GU 4990-104.

REFERENCES

Babour, K., and Mosnier, J., 1979, Differential geomagnetic sounding in the Rhine graben: Geophys. J. Roy. Astr. Soc., **58**, 135–144.

Berdichevskiy, M. N., and Dmitriev, V. I., 1976, Distortion of magnetic and electrical fields by near-surface lateral inhomogeneities: Acta. Geodaet. Geophys. et Montanist., Hungarian Acad. Sci., **11**, 447–483.

Cagniard, L., 1953, Basic theory of the magnetotelluric method of geophysical prospecting: Geophysics, **18**, 605–635.

Cantwell, T., 1960, Detection and analysis of low frequency magnetotelluric signals: Ph.D. thesis, Mass. Inst. Tech.

Fisher, G., Schnegg, P. A., Peguiron, M., and Le Quang, B. V., 1981, An analytic one-dimensional magnetotelluric inversion scheme: Geophys. J. Roy. Astr. Soc., **67**, 257–278.

Gamble, T. D., Goubau, W. M., Miracky, R., and Clarke, J., 1982, Magnetotelluric regional strike: Geophysics, **47**, 932–937.

Hermance, J. F., 1982, The asymptotic response of three-dimensional basin offsets to magnetotelluric fields at long periods: The effects of current channelling: Geophysics, **47**, 1562–1573.

Johansen, H. K., 1977, A man/computer interpretation system for resistivity soundings over a horizontally stratified Earth: Geophys. Prosp., **25**, 667–691.

Jupp, D. L. B., and Vozoff, K., 1975, Stable interactive methods for the inversion of geophysical data: Geophys. J. Roy. Astr. Soc., **42**, 957–976.

Larsen, J. C., 1975, Low-frequency (0.1-6 cpd) electromagnetic study of the deep mantle electric conductivity beneath the Hawaian Islands: Geophys. J. Roy. Astr. Soc., **43**, 17–46.

Le Mouel, J. L., and Menvielle, M., 1982, Geomagnetic variation anomalies and deflection of telluric currents: Geophys. J. Roy. Astr. Soc., **68**, 575–587.

Parker, R. L., 1980, The inverse problem of electromagnetic induction: existence and construction of solutions based on incomplete data: J. Geophys. Res., **85**, 4421–4428.

Parkinson, W. D., 1962, The influence of continents and oceans on geomagnetic variations: Geophys. J. Roy. Astr. Soc., **6**, 441–449.

Pedersen, L. B., 1979, Constrained inversion of potential field data: Geophys. Prosp., **27**, 727–748.

——— 1982, The magnetotelluric impedance tensor—Its random and bias errors: Geophys. Prosp., **30**, 188–210.

Ranganayaki, R. P., 1984, An interpretative analysis of magnetotelluric data: Geophysics, **49**, 1730–1748.

Sheffe, H., 1959, The analysis of variance: Wiley.

Sims, W. E., and Bostick, F. X., 1969, Method of magnetotelluric analysis: Res. Lab. tech. rep., **58**, Univ. of Texas-Austin.

Wannamaker, P. E., Hohmann, G. W., and Ward, S. H., 1984, Magnetotelluric responses of three-dimensional bodies in layered earths: Geophysics, **49**, 1517–1533.